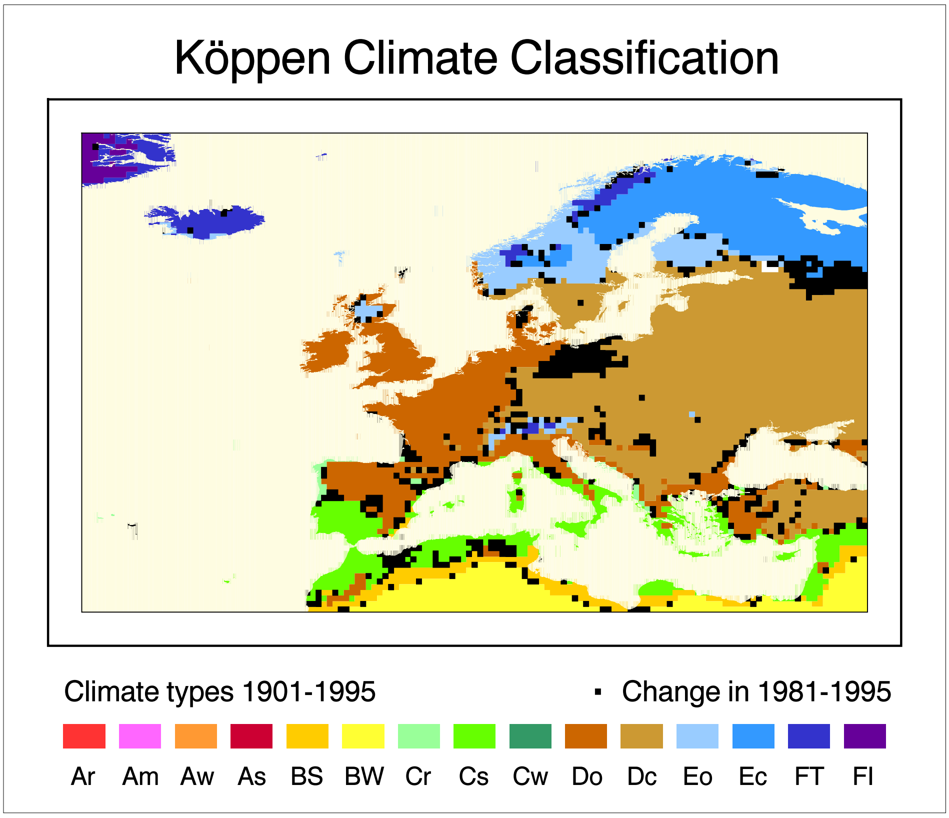
Köppen Climate Classification
Climate types 1901-1995
▪ Change in 1981-1995
Ar
Am
Aw
As
BS
BW
Cr
Cs
Cw
Do
Dc
Eo
Ec
FT
FI

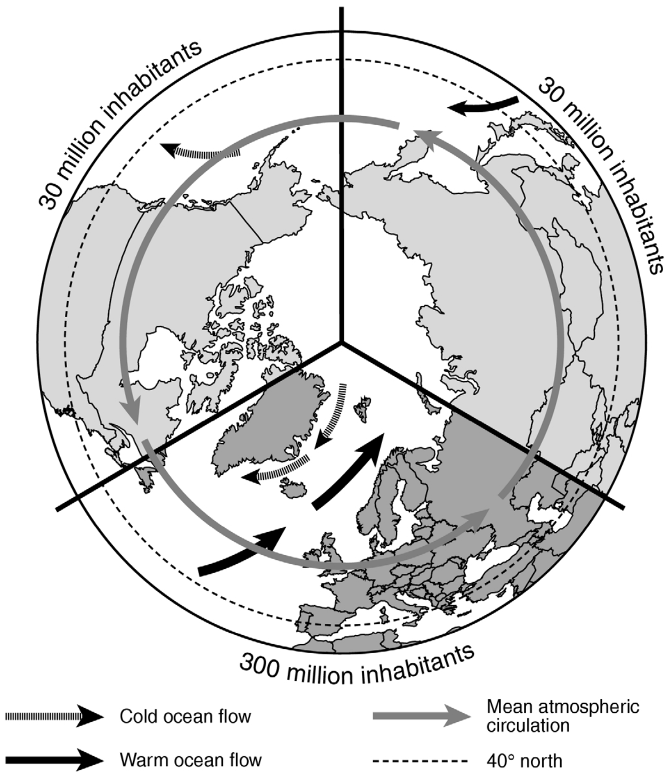
30 million inhabitants
30 million inhabitants
300 million inhabitants
Cold ocean flow
Warm ocean flow
Mean atmospheric circulation
40° north

1. Space-Time Variability of the European Climate*

Klaus Fraedrich and Christian-D. Schönwiese

Abstract: Observational data sets are analyzed in four steps to provide a comprehensive view of climate and climate variability in Europe. The *first* step towards an overall description of climate is the analysis of the spatial distributions of means and variances of basic climate elements (surface air temperature, sea level pressure, and precipitation). The *second* step identifies the climate generating dynamical processes; here, cyclone paths and storm tracks provide climatologies from quantitative Lagrangian and Eulerian analyses of weather data; Grosswetterlagen and climate zones, on the other hand, represent climatologies based on qualitative patterns (regimes) embedding the climate into its geographical and biospheric environment. A *third* step of analysis is necessary because these climatologies indicate recent climate changes at the end of this century. This is documented in terms of the spatial distribution of time averaged climate elements and of various measures of their variability (see preceeding steps). The *fourth* step evaluates the causes of the observed trends analyzing the effects of external forcing (volcanism, solar, and anthropogenic) by empirical methods.

* From *The Science of Desasters: Climate Disruptions, Heart Attacks, and Market Crashes* (Springer Verlag, 2002), A. Bunde, J. Kropp and H.J. Schellnhuber (eds.)

◄ **Fig. 1.0. Top:** Climate zones in Europe (1901–1995) and their shifts in the period 1981–1995 (in black): tropical (A), dry (B), subtropical (C), temperate (D), boreal (E), snow (F) with tundra and perpetual frost (T, I). **Bottom:** Climate related living conditions in three sectors of the northern hemisphere north of 40°N, (after Krauß and Augstein 1991, from WBGU 1998)

1.1 Introduction

Climate describes the relatively long–term behavior of the climate system whose components comprise the atmosphere, the hydrosphere (ocean and fresh water of land areas), the cryosphere (land and sea ice), the pedosphere, the lithosphere (both representing the land surface) and the biosphere (especially vegetation). This system is observed specifying the space–time variations of climate elements like temperature, air humidity, precipitation, air pressure, wind, cloudiness etc. most of them characterizing the subsystem atmosphere. Information from prehistorical time is provided by reconstructions (paleoclimatology). Consequently, climate is described using proper statistics of all types of variability and for all relevant space–time scales. This variability is forced by internal interactions within the climate system and external influences. Related process studies and modeling may lead to an understanding of the climate system behavior, which includes deterministic and statistical modeling and verification against observations.

Climate and climate change gain public interest for the following reasons: (i) Human welfare can be linked to climate variability and, in the future, mankind may also benefit or suffer from natural or anthropogenically induced climate variations. (ii) In historical and, much intensified, in industrial time mankind is becoming a climate forcing factor, so that climate protection (UN Framework Convention on Climate Change) appears to be an urgent task.

The scientific knowledge about climate and climate variability is still incomplete: The climate data base, the understanding of the processes participating in climate change, and the role of the anthroposphere with its socio-economic response as a feedback process. Future scenarios and predictions of the climate system have an extremely important presupposition: Description and understanding of past climate variability need to be both as exact and comprehensive as possible. This requires intensive cooperation of scientists.

As a contribution to the very basis of this task, that is the awareness of our present knowledge, some aspects of space–time statistics of climate variability are systematically addressed focusing our attention on Europe. Time and space scales are discussed (section 1.2); we deal with the quantitative and qualitative measures of climate (section 1.3, step one and two of the climate analysis) in terms of means and variabilities, including storm tracks, cyclone paths, Grosswetterlagen and climate zones. Finally, trends of these measures are presented and the effects of external forcing are discussed (section 1.4, step three and four of the analysis).

1.2 Time and Space Scales: Peaks, Gaps and Scaling

In each climate compartment the life–span and intensity of the largest energy containing eddy characterizes the predictability and variability in terms of the decay period of a perturbation. Useful estimates of their memories and predictabilities can be obtained from the residence times of water as an important carrier of latent energy (Tab. 1.1). The observed large differences of the memories of the interacting systems challenge monitoring and modeling of climate variability.

Sub–systems	time–scales
Atmosphere	< 10 days (weather)
Ocean/Land	1 month (upper layers) to 10^3 years (deep ocean)
Cryosphere	< 10 years (sea ice) to $> 10^3$ years (ice shields)

Table 1.1. Time–scale estimates.

The scale range of atmospheric phenomena, for example, spans from raindrops to planetary waves in space and covers events between very short turbulent outbursts and climate change. Power spectra of time series of climate observables, their extrema and power–law slopes (Fig. 1.1) provide further information on the climate dynamics and variability.

Spectral *maxima* (or peaks) represent dominating time scales. Such peaks occur in the following period–bands: 12 and 24 hours (diurnal and half–daily cycle), 3 days to one month (weather variability ranging from turbulent eddies to planetary waves), half–annual and annual cycle, the quasi–biennial oscillation (QBO) of the tropical stratosphere, the El Niño/Southern Oscillation (ENSO) (3–7 years), solar cycles (10–20 years), 100–1 500 years (little ice age like events), 22, 41 and 100 thousand years (astronomical cycles) and, finally, geological scales related to orogenesis and continental drift. An idealized spectrum of a time series of a hypothetical climate element is presented in Fig. 1.1.

Spectral *minima* (or gaps) identify periods useful for time–averaging and sampling (see, Fig. 1.1a, points 1–4): These averaging periods range from a 3 hour time scale, which characterizes synoptic sampling, via monthly periods describing the march of the seasons and intra–annual variability, to decadal periods, which correspond to climate fluctuations, while million years represent tectonic changes.

Spectral *scaling* characterizes the non–linearity of atmospheric dynamics. A scale range, which exhibits scale invariance relates fluctuations at smaller scales to those of larger ones by the same power law scaling without preferred mode of excitation. In this sense, a power law or scaling behavior within a frequency band

$$S(\omega) \sim \omega^{-b} \tag{1.1}$$

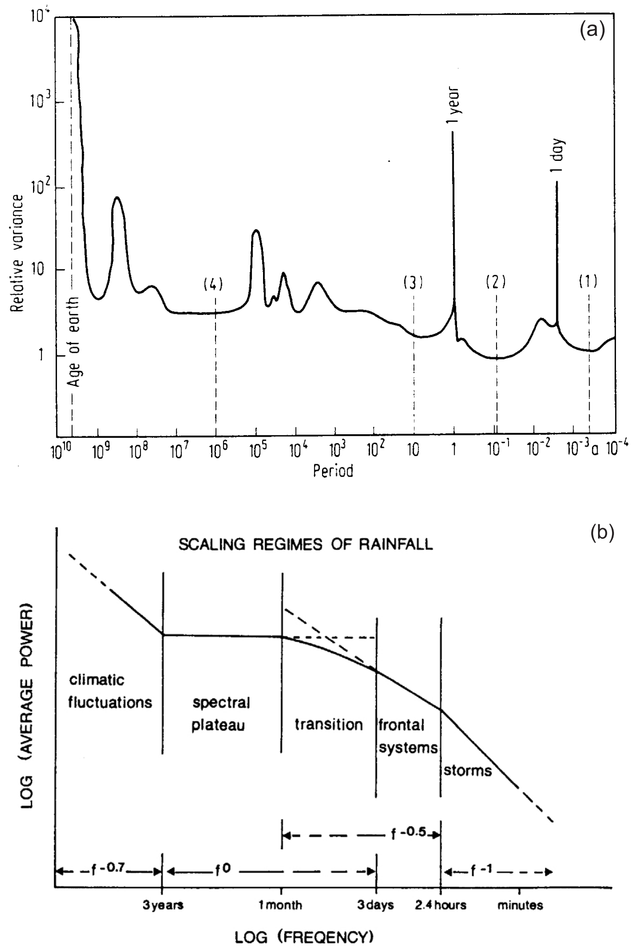

Fig. 1.1. Spectra of climate variability: (a) Schematic climate spectrum [1.50, 1.43]; spectral maxima represent dominant atmospheric and climatic phenomena and their associated period; spectral minima (points 1-4) identify periods of time-averaging. (b) Schematic scaling regimes of continental European rainfall [1.17]; spectral power law scaling (scale invariance) characterises the non-linear dynamics of regimes of atmospheric variability.

is another characteristic of the variability of the dynamical system (Fig. 1.1 b). Analysis of rainfall at European stations reveals a regime of climate fluctuations ($b \sim 0.7$) for periods > 3 years; this differs from the $b \sim 2$ red noise power law spectrum connecting the level of small scale white noise forcing with that of the white large scale response. A spectral plateau $b \sim 0$ represents variability of the large scale circulation (3 years to 1 month) which is linked through a transition zone with a regime of frontal systems ($b \sim 0.5$, lasting less than 3 days). The break at 2.4 hours and the standard meteorological interpretation of the associated meso–scale regime remain an open question.

1.2.1 Time Scales: Power Spectrum Analysis

Power spectrum analysis transforms any time series, e.g. of climate elements like temperature or precipitation, into a spectrum where the contributions of variance are related to a particular sequence of frequency or period bands, respectively. Spectral peaks point to possible cyclical variance components whereas the background spectrum, especially its behavior in respect to low frequencies, reveals whether the process implies persistence (leading to so–called "red noise") or not ("white noise").

There are a number of algorithms available providing spectral density estimates (see e.g. [1.42,1.64]). The easiest way is to compute the Fourier transform of the autocorrelation function, called autocorrelation spectrum analysis (ASA). Corresponding confidence tests (χ^2–test) are available and easy to handle. An alternative method is based on the information entropy theory and called maximum entropy spectral analysis (MESA). Compared to ASA it reveals a better resolution of the frequency bands (especially at low frequencies) but involves confidence test problems. The singular spectrum analysis (SSA) is again, like ASA, based on the computation of the auto-covariance matrix but introduces an EOF (empirical orthogonal function) transformation by the computation of the eigenvalues of this matrix. In this case it needs to be decided for all EOFs whether the confidence intervals of the eigenvalues overlap. Then the related frequencies are isolated using ASA or MESA estimates. In addition, wavelet analysis is some type of a combination of spectral analysis and numerical filter techniques where these filter techniques themselves are able to suppress variations within the relatively high–frequent part of the spectrum (low–pass filter) or low–frequent part (high–pass filter) or both, so that a particular frequency band remains (band–pass filter). Usually, the result is shown in terms of the filtered time series.

As an example, the annual surface air temperature variations 1758–1998 at Frankfurt/Main (Germany, see Fig. 1.2a) is shown including the 10 year low–pass filtered (smoothed) data suppressing variations of periods $< 10yr$. Because of an observation gap and some uncertainties in earlier years we use only the period since 1857. ASA and MESA, see Fig. 1.2b, indicate some peaks where in case of ASA only two peaks exceed the 90% confidence level, 2.1 and 2.3 yr (quasi–biennial oscillation), whereas in case of MESA the most prominent peak is 7.8 yr although a pronounced 2.3 yr peak is also indicated. It should be mentioned that an approximately 8 yr peak is also found in the time series data of the North Atlantic Oscillation (NAO). ASA shows a "red noise" background spectrum with variance increasing towards low frequencies/long periods, which is reflected in the confidence level; MESA does not. Figure 1.2c shows the result employing SSA analysis. Note that the eigenvalue (95%) confidence intervals of the first two EOFs do not overlap with the other. A MESA of these first two EOFs indicates a 7.6 yr cycle, which is close to the dominant MESA peak of the original time series. The eigenvalues of the first two EOFs are almost identical indicating a harmonic oscillation.

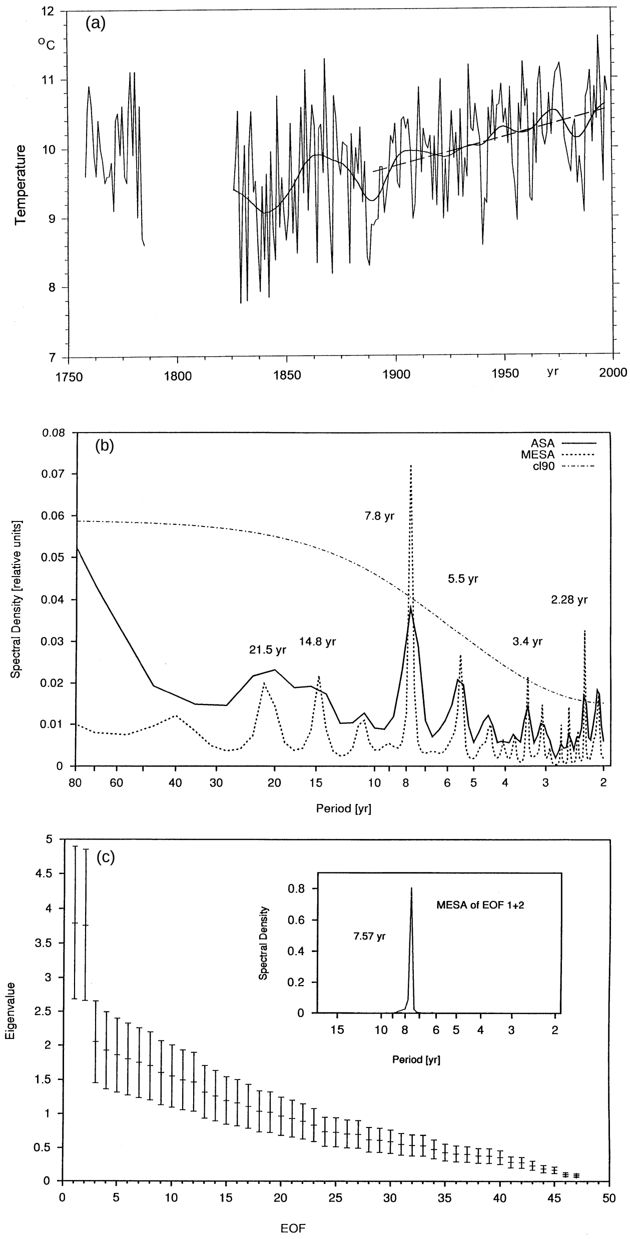

Fig. 1.2. (a) Observed annual surface air temperature variations 1758-1998 (observation gap 1786-1825) with 10 yr low-pass filtered data (smooth line) and +1.1K linear trend (dashed line) at Frankfurt/Main, Germany (1850-1998). (b) Related power spectrum analysis 1857-1996 (ASA = autocorrelation spectrum analysis, MESA = maximum entropy spectrum analysis, cl90 = 90 percent confidence level). (c) Related singular spectrum analysis (SSA) including MESA of EOF1 + EOF2.

1.2.2 Space Scales: Correlations and Representativeness

Climate time series statistics varying in space are represented by their correlations from station to station or grid point to grid point. This leads to information about the number of stations or grid points necessary to derive proper space–related statistics. An example may illustrate this problem. Figure 1.3a (from Malcher and Schönwiese [1.39]) shows a relationship where, related to the nordic station Helsinki (1881–1980), the annual surface air temperature time series correlation coefficients (linear Pearson correlation) are plotted against the station distance (182 stations considered, 114 from Europe); confidence levels 90% – 99.9% are also indicated. It appears that these correlations drop to values < 0.7 (corresponding to about 50% of the common variance) approximately at a distance of 1 000 km and that even at a 2 000 km distance correlations are still significant. At a distance of 6 – 8000 km, correlations turn again positive (and significant); these teleconnections are related to the rain-bearing frontal systems which, associated with the Rossby wave pattern of the atmospheric circulation, dominate Europe's climate. Mean sea level pressure shows a similar behavior (see Schönwiese and Rapp For summer precipitation, however, correlations drop to values < 0.7 at distances near 50 km, Fig. 1.3b, (for 250 stations surrounding Frankfurt/Main, 1891–1990; [1.53]). In winter the correlation distance changes to about 200 km. These distance numbers are a measure of representativeness: In case of temperature and pressure (large numbers) we have a fair representativeness and do not need so much information in space; this, however, is not the case for precipitation (small numbers). Note, that the typical representativeness distance defined by any reasonable correlation range does not only depend on climate elements and seasons but

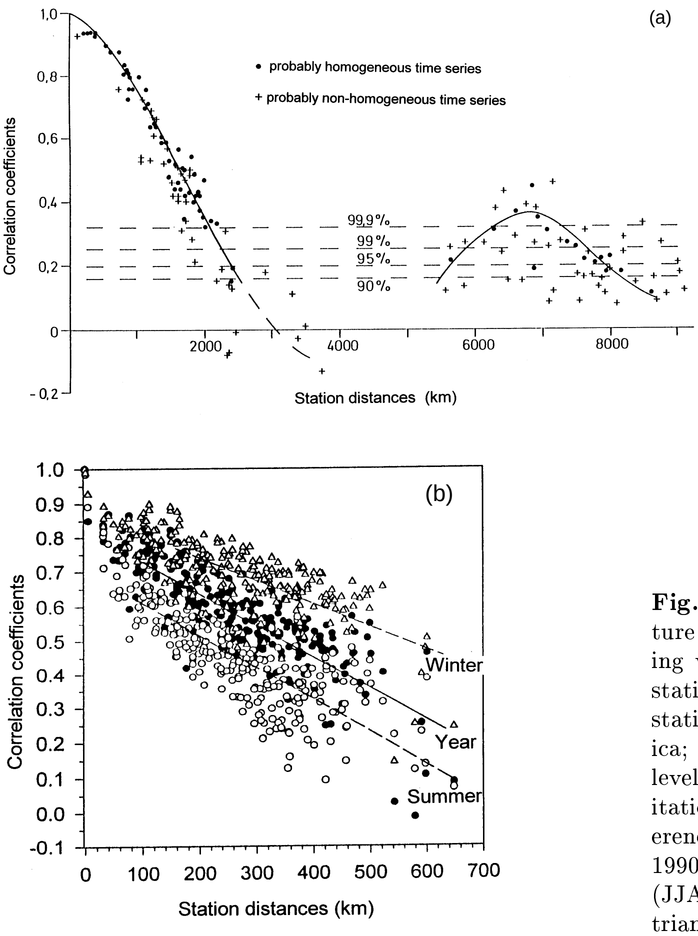

Fig. 1.3. (a) Surface air temperature correlations (1881-1980) changing with distances between reference station Helsinki (Finland) and other stations in Europe and North America; dashed lines specify confidence levels [1.39]. (b) As (a) but for precipitation correlations in Germany (reference station Frankfurt/Main, 1891-1990): annual (full circles), summer (JJA, open circles) and winter (DJF, triangles) [1.53].

also on the data resolution in time and on the climate regime. Moreover, there are also long–term changes associated with Grosswetter or climate trends. The subsequent analysis of climate variablity is extended deriving the degrees of freedom of Grosswetterlagen and climate zones.

1.3 Europe's Climate: Storm Tracks, Grosswetterlagen and Climate Zones

Weather and climate observations are analyzed to obtain quantitative physical information in terms of energy and momentum budgets of the atmospheric dynamics, their space and time filtered properties in the space–time or wavenumber–frequency domain, and nonlinear interactions. Regional climates and the associated variability are described by spatial distributions of time means and anomalies. Another type of data analysis which is qualitative or phenomenological, identifies and describes structurally stable patterns. That is, large scale circulation systems which are related to real weather (highs and lows) processes or climate zones (associated with typical biota). Both types of analysis describe the same physical processes but contribute different aspects to it. For both approaches to represent climatologically meaningful space–time behavior, the underlying quantitative data sets have to be subjected to prior determination of the spatial degrees of freedom (or dimension) in order to substantiate the number of phenomenological patterns selected for the analysis: The linear approach is based on the superposition of independent modes and leads to estimates of the spatial degrees of freedom; the non–linear method of scaling is more dynamically oriented. This section presents a description of European climate in terms of its space–time variability which is based on suitable physical and phenomenological data sets; climate change issues are addressed in the subsequent section.

1.3.1 Climate Means and Variability Patterns: Pressure, Temperature and Precipitation

The local surface climate at a grid point or single station is conventionally described by three variables (climate elements), which imply a suitable time average (say, a winter month) $C(t) = (P, T, N)$: the monthly mean sea level pressure P, temperature T, and precipitation N. Variability is suitably described by anomalies $C(t)' = (C(t) - \langle C \rangle)/\sigma_i$, from the long term ensemble mean of, say, thirty years $\langle C \rangle$, and which are normalized by the respective standard deviations, σ_i. In this sense the North Atlantic/European climate is represented by the fields of the ensemble means $\langle C \rangle$, while the space–time variability is comprised in the remaining anomalies $C'(t)$. The information in

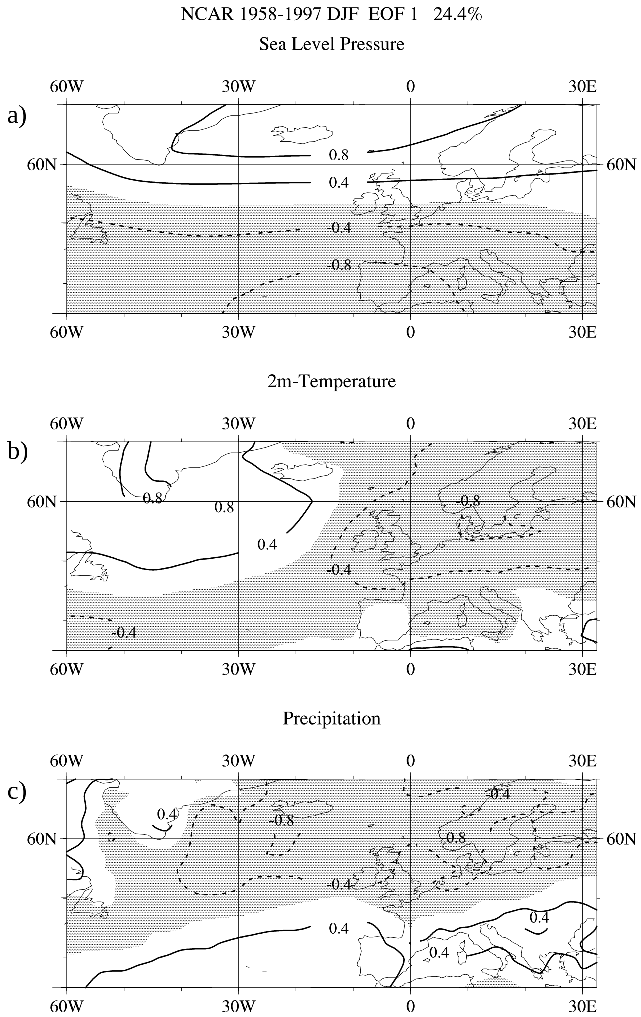

Fig. 1.4. Joint spatial variability of the winter climate in the North Atlantic/European sector (winter seasons 1958-1997): The dominating EOF1 describes the North Atlantic Oscillation (NAO) in terms of (a) montly mean sea level pressure P, (b) temperature T and (c) precipitation N.

this anomaly data set can be suitably reduced by empirical orthogonal function (EOF) analysis which separates the space and the time variability. The eigenvectors of the covariance matrix of the anomalies describe spatial patterns which are commonly ranked by their contribution to the total variance (denoted by their eigenvalues). These North Atlantic/Europe eigenvectors (see, Kutzbach [1.35] for a climate analysis of North America) represent contributions to regional climate anomalies containing information on the simultaneous distribution of the sea level pressure, temperature and precipitation. They are used to reconstruct the original anomaly state vector by their respective principal components (PCs or amplitudes $E1(t), E2(t)$, ...).

Space and time variability (North Atlantic Oscillation): Forty years of NCAR (National Center for Atmospheric Research) re–analyses (1958–1997, representing the synoptic scale with a 250 km resolution) reveal a dominating eigenvector, EOF1, which contributes almost a quarter (24.4%) to the total variance. Its spatial pattern provides a first indication that precipitating frontal systems determine the variability of the North Atlantic/European climate (Fig. 1.4). The following two describe 14.3% and 11.9% of the variance (not shown), so that a hypothetical degeneracy of EOF2 and 3, whose eigenvalues should differ by the estimated standard deviation of either cannot be excluded (see North et al. [1.47]).

EOF1 reveals a marked north–south anomaly pressure difference between Iceland and the Azores/Iberian Peninsula, which is known as the North Atlantic Oscillation (NAO). It represents, for positive NAO index, an enhanced zonal flow across the North Atlantic, which is associated with a deep Iceland low and a strong Azores high generating higher (lower) temperatures and more (less) precipitation over the eastern (western) part of the North Atlantic and northern (southern) parts of the European continent. These situations influence the climate variability between Newfoundland and the Black Sea.

The other EOF's (not shown) modify the EOF1–variability; EOF2, for example, represents situations with enhanced anticyclonic "Grosswetter" over the European continent, which are associated with a shift of the tail end of the cross–Atlantic storm track. In low pressure situations, a negative pressure anomaly extends over the European continent. The related more southward position and zonally oriented cyclone track is associated with frontal systems which lead to enhanced precipitation and positive temperature anomalies in the central and southern parts of Europe.

As the European climate is dominated by the North Atlantic Oscillation (NAO), it is not surprising that suitable NAO circulation indices are subjected to climate change analysis. These are the PCs of the dominating first EOF of the surface pressure or combined fields projecting the vector time series C_i(t) onto the EOF or eigenvectors, or simply the pressure difference between stations on the Azores and on Iceland. About hundred years of observations show the following results: (i) The first combined EOF indicates a significant bimodality (see Fraedrich et al. [1.16]). (ii) The observed NAO station index varies on interannual up to interdecadal time scales, indicating non-stationarity of the NAO (Fig. 1.5). A standard wavelet analysis exhibits active and passive NAO phases with low and high frequency variability, respectively. The hemispheric circulation during the *active* phase is dominated by the North Atlantic Oscillation, whose index fluctuates with periods between 15 and 7 years, shows enhanced low-frequency variability and large extremes (see Appenzeller et al. 1998 and, for the 1962-76 winter months, Wallace and Gutzler 1981). The *passive* phase reveals a minimum in low-frequency variability characterized by enhanced variance on shorter time scales (about 4 year period). The hemi-

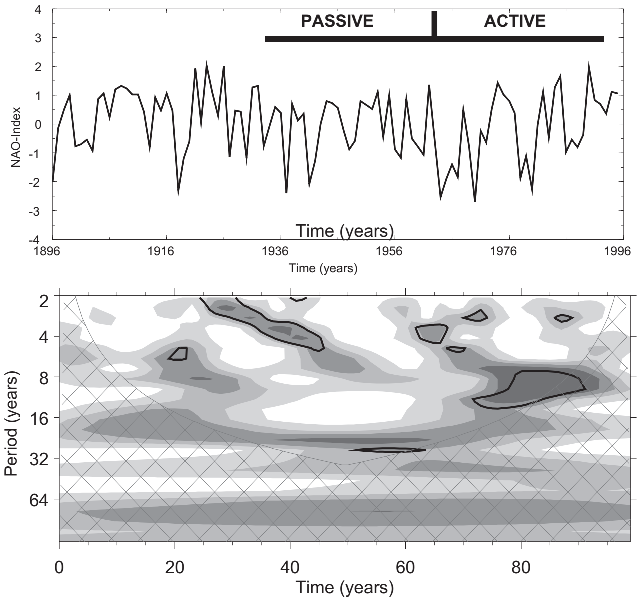

Fig. 1.5. North Atlantic Oscillation index time series (top, winter mean surface pressure differences Azores minus Iceland; Hurrel [1.28]) and wavelet power spectrum (bottom).

spheric circulation is dominated by the Pacific/North America teleconnection pattern (PNA); it evolves in the tropical/subtropical Pacific and has a strong influence on the southwestern part of the North Atlantic (exciting the Aleutian Low and the North American High).

Extrema: The analysis so far is confined to the first and second moments (means and variances) and needs to be extended to higher moments or, equivalently, to the complete probability distribution, in order to obtain additional information about its intensity fluctuations, in particular extrema or intermittency (and thus the higher moments). They are represented by the tail end of the cumulative distribution. For example, the 5–min rainfall totals, N, of a single station (Potsdam, Germany) reveal the following structure (Fig. 1.6, [1.17]). The linear drop of the tail end of the probability distribution is not approached smoothly from the curve of the "bulk" of the distribution, but rather abruptly as a break from the rest of the distribution. Quantitatively, this tail, if approximated by a power law of the type

$$F(N) = \text{Prob}\ \{N > n\} \sim n^{-a}, \tag{1.2}$$

shows a lesser reduction in probability for increasing intensity fluctuations in the 1 mm to 2 cm regime ($a \sim 1.7$), than for intensities $>$ 2 cm ($a \sim 3.0$). That is, the recurrence time (or return period) of the same hypothetically large event is shorter for the smaller power law slope (and vice versa). For example: an event $>$ 10 cm, which occurs with probability 10^{-6} in the $a \sim 3.0$ regime, would, in the a $\sim$ 1.7 regime, occur with probability 10^{-5} and thus return an order of magnitude earlier, a more pessimistic scenario.

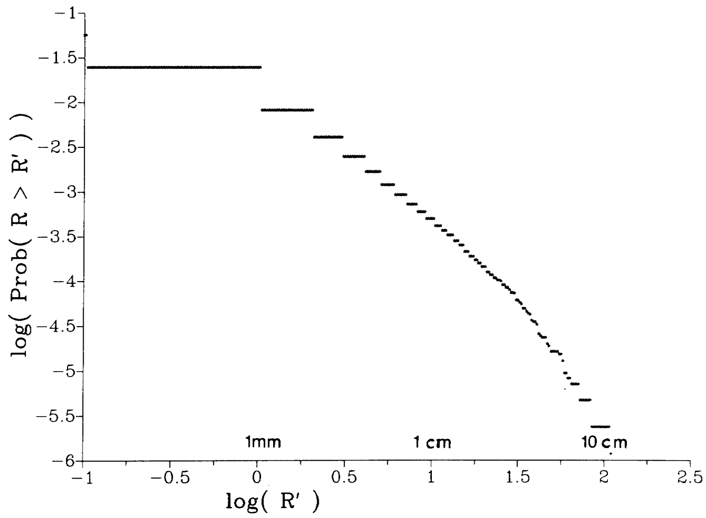

Fig. 1.6. Probability distribution of rainfall in a log-log diagram: Single station (Potsdam, Germany) 5–min data, which are distribution averaged over eight summers (after Fraedrich and Larnder [1.17]).

A *biased coin flip* model is the basis of this analysis of the probability distribution [1.25]. Here, the continuous rainfall variable is subjected to dichotomy utilizing the occurrence of observations smaller than the fixed rainfall threshold $n : q = 1 - F(n) = \text{Prob}\ \{N < n\}$. A subsequent Bernoulli experiment determines the first exceedance of the threshold p at the j–th trial; its outcome is the geometric distribution, $\omega(j) = Fq^{j-1}$, with mean $\langle j \rangle = \tau = 1/F$, and standard deviation $s = (\tau^2 - \tau)^{1/2}$. Multiplying by the sampling time, the mean, $\langle j \rangle = \tau$, defines the expected return period of (the occurrence of) an intermittent event (that is, threshold exceedance or $N > n$), for which to happen once, $\tau = 1/F$ trials are necessary in the average; if n is the median, then the event $N > n$ returns on the average every second trial, $\tau = 2$; if n is the upper quartile: $\tau = 4$, etc.

1.3.2 Storm Tracks and Cyclone Paths: Eulerian and Lagrangian View

As indicated by the eigenvector analysis, synoptic weather systems form an integral part of the space–time variability of European climate. They undergo a life cycle during which they follow more or less well defined paths known as cyclone or storm tracks; they are associated with rainbearing frontal weather systems affecting regional climates, in particular, the water cycle and extreme weather events. The European weather and climate is affected by the variability of the cross Atlantic cyclone track, in particular by its sensitive tail, which is associated with the final stages of a cyclone's life cycle. About 70–80% of the winter precipitation in continental Europe originates from about 15 frontal cyclones based on single station (Berlin) composite analysis (Fraedrich et al. [1.19]). These storm tracks can also be influenced by distant atmospheric

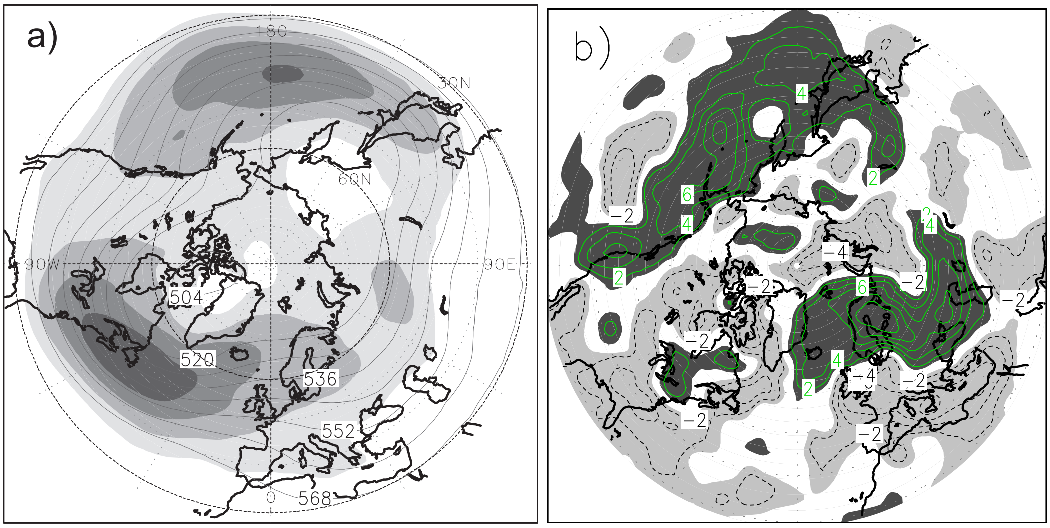

Fig. 1.7. Storm track (1979-1997): (a) The r.m.s. of the 500 hPa band pass filtered geopotential height anomaly; the climatological distribution of the winter 500 hPa height averages (in gpdm) is also included. (b) The decadal trend of the storm track. The contour intervals of the stippled area are (a) 10m, (b) 2m, dark shade denotes positive, light shade negative anomalies (after Sickmöller et al. [1.56]).

events, like the ENSO system in the tropical Pacific (see, for example, [1.16]). Furthermore, relatively fast fluctuations in the North Atlantic storm track interact with the oceanic conveyor belt through the freshwater flux (or rainfall) possibly leading to low frequency variability in the ocean and, likewise, in the atmosphere. Space–time variability of atmospheric dynamics is conveniently described by Eulerian statistics of model or observational data sets to comprise the physical information contained in the sequence of weather maps. The height (or geopotential) of a pressure surface is traditionally used to describe mid–latitude synoptic scale systems.

Storm tracks: The storm track is a common measure for the mean intensity of mid–latitude disturbances. It is defined as a region with enhanced standard deviation of the variability of the band–pass filtered (2.5–6 days) 500 hPa geopotential height to identify regions of strongest baroclinic activity (Lau [1.37]). The axis of the storm track is located along the jet–stream as determined in the 500 hPa geopotential height. There are two distinct regions recognized over the oceanic basins of the Northern Hemisphere with a magnitude of 60 m (Fig. 1.7a, deduced from the European Center for Medium Range Weather Forecasting, ECMWF, re–analyses; [1.56]): The North Atlantic and North Pacific. The North Atlantic storm track is considerably stronger and extends from the centre of the North American continent to Northern Europe, whose climate is considerably affected by the eddy activity of these synoptic scale systems; the Pacific storm track is restricted to the ocean.

Cyclone paths (scaling and climatology): The cyclone track is the region of an enhanced density of synoptic cyclones. The comparison between storm track and cyclone track reveals some discrepancies: anticyclones are included in the statistics defining a storm track, and its variability is not confined to geopotential height minima [1.65]. For example, the occurrence of minima in the superposition of a wave with a zonal flow depends on the flow intensity, whereas the variability depends on the wave only. Cyclone paths are sensitive to the particular tracking method; they are identified subjectively or by a search algorithm (as, for example, developed by Blender et al. [1.7]), the simplest of which consists of two steps: (i) A cyclone is detected as surface pressure low and therefore as a local minimum from the 1 000 hPa reference field in an area covering 3×3 grid points. (ii) A sufficient intensity of the low requires a positive mean gradient of the 1 000 hPa height over an area characterized by the Rossby deformation radius (1 000 km). The trajectory $X_j(t)$ of the individual cyclone j is a sequence of cyclone positions $(x_j(t), y_j(t))$ for 6 hourly time steps $t = 0, \ldots, T = 3$ days; the high temporal resolution is required to guarantee the cyclone traces of the sequentially identified lows. Cyclone locations are further analyzed relative to their initial position, $dX_j(t) = X_j(t) - X_j(t = 0)$,

$$X_j(t = T) = \Big[x_j(t = 0), y_j(t = 0); ...; x_j(T), y_j(T)\Big] \text{, } and \tag{1.3}$$

$$dX_j(t = T) = \Big[dx_j(t = 0), dy_j(t = 0); ...; dx_j(T), dy_j(T)\Big] \text{,} \tag{1.4}$$

where eqs. 1.3 and 1.4 indicate the cyclone and its relative track. Formally, the trajectory or the relative displacement of an individual cyclone is characterized by a single point in a time–delay coordinate phase space spanned by the consecutive (relative) cyclone positions. Applying cluster analysis to this phase space leads to three dominating centroids of mean relative displacement, which represent Lagrangian–type regimes of stationary, north–eastward and zonally traveling cyclones (see Fig. 1.8. The latter two centroids correspond to the extremes of the North Atlantic Oscillation (NAO) which characterizes the Iceland low and Azores high see–saw and is associated with low frequency (decadal) variability (see section 1.3.1). An ensemble averaged ($\langle\rangle$) position of the propagating cyclone clusters and the life–cycle of the horizontal pressure gradient are shown in Fig. 1.8a,b.

Cyclone track scaling or, more generally, scaling in ocean and atmosphere dynamics originates from diffusion processes. In this sense Fraedrich and Leslie [1.20] adopt Richardson's experiment [1.49] and analyze tropical and mid–latitude cyclones (for a review see [1.61]). Treating traveling cyclones as large scale diffusive elements, they obey a fractional power–law scaling of the time behavior of the mean square displacements, $dX^2(t) = dx^2(t) + dy^2(t)$ (normalized by standard deviations). This leads to the structure function which,

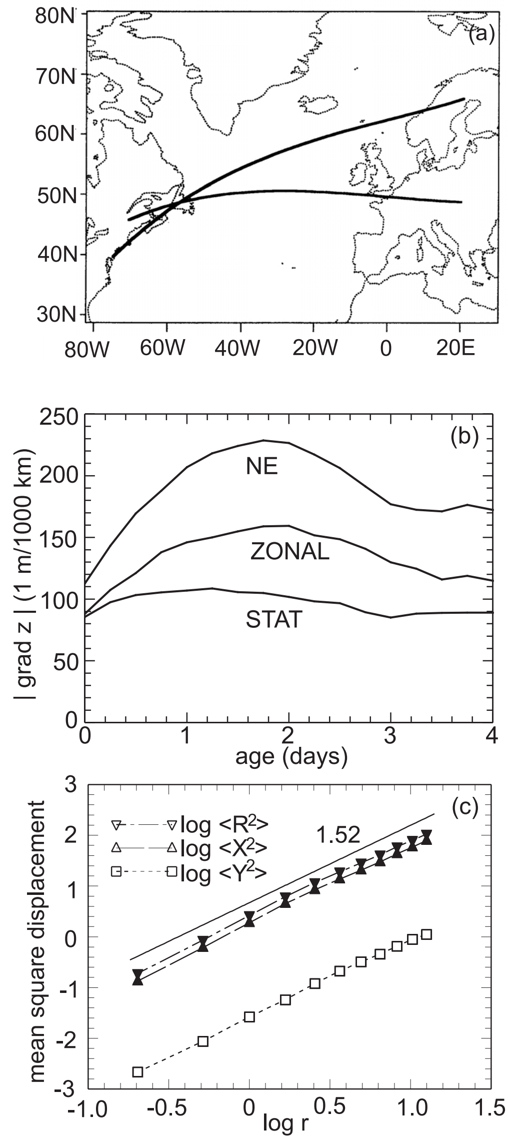

Fig. 1.8. Paths of North Atlantic cyclones: (a) Mean trace of cyclone positions in the north–eastward and zonal clusters; (b) the average life cycle of the 1 000 hPa height gradient, and (c) their scaling (after [1.7]).

for stationarity, corresponds to a power law spectrum:

$$\langle dx^2(t) + dy^2(t)\rangle \sim t^q. \tag{1.5}$$

For geophysical flows $1 < q < 2$ is observed. The mean square displacement is calculated for the whole set of cyclones and for the different clusters. Figure 1.8c shows a power law scaling of the total, zonal, and meridional displacements of the cyclones in the North Atlantic/European sector in log–log format: $\langle dx^2 + dy^2\rangle$, $\langle x^2\rangle$, $\langle y^2\rangle$ for the upper, middle and lower curves. The average of all cyclones yields $q \sim 1.52$, the (north–eastward $q \sim 1.67$, zonal $q \sim 1.59$). The stationary cyclones follow purely diffusive behavior with $q = 1$. The results for the zonal and north–eastward propagating cyclones can be compared with

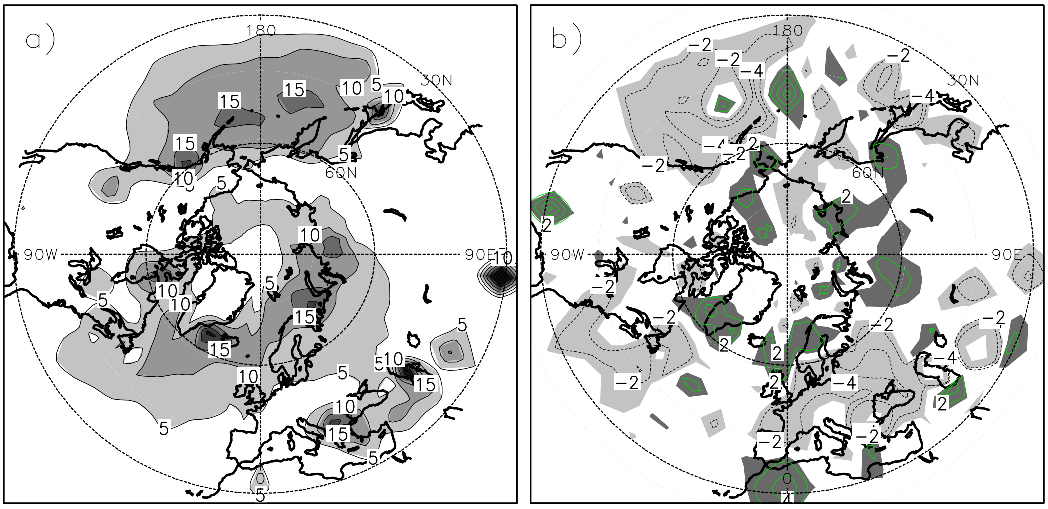

Fig. 1.9. Cyclone density (1979-1997): (a) Occurrence and (b) decadal trend. The density gives the ratio (times 100) of an occupation of 1 000 km^2 by cyclones at an observation time. Contour intervals are 5% in (a), 2% in (b). The trend in (b) is positive for dark shade, negative for light shade (after [1.56]).

$q \sim 1.67$ of a simple point vortex model for the mid–latitude circulation [1.63]; ocean drifter trajectories follow $q \sim 1.5$ [1.51]. This behavior, observed in many geophysical flows, characterizes a trajectory of fractal or self–similar dimension $d = 2/q$; that is, cyclone motion is neither purely linear ($q = 2$) nor diffusive ($q = 1$).

A *cyclone climatology* is provided by cyclone densities following Köppen's [1.34] first analysis of North Atlantic/European cyclone paths. The 1979–97 cyclone density (Fig. 1.9a, see also Sickmöller et al. [1.56]) shows the temporal occupation of cyclones per 1 000 km^2. The cyclone trajectories are mainly located in the storm track area; they originate over the western parts of the oceans and travel eastward bending northward until the end of their life cycles. The cyclone density reaches 0.1 in the storm track areas. Similar to the storm track, the cyclone density over the North Atlantic extends westwards onto the American continent. Distinct density maxima within the storm tracks are found southeast of Greenland in the Denmark Strait, in the Barents Sea, the Canadian Sea, and the Gulf of Alaska. Further maxima are detected in the Mediterranean Sea. Cyclogenesis is located in the baroclinic zones at the western or upstream parts of the storm tracks. While the North Pacific cyclones arise over sea, North Atlantic cyclones originate partly over the North American continent; the Mediterranean and the Caspian Sea are other regions of cyclogenesis. There are areas of secondary cyclogenesis east of Greenland and over northern Europe. Cyclolysis occurs in the north–eastern end of the storm tracks with pronounced maxima in the Gulf of Alaska and the Denmark Strait. Secondary cyclones over northern Europe end in the Arctic sea while the Mediterranean cyclones end in south–eastern Europe.

1.3.3 Grosswetterlagen and Climate Zones

Early analyses of weather and climate were based on phenomenological classifications of the underlying synoptic scale processes and of the climatic zones realizing that large scale patterns of recurrent weather episodes or of vegetation–climate coherences are fundamental properties of the atmosphere and the climate system. Before utilizing these phenomenological data sets (types of Grosswetterlagen or climate zones) for further statistical analysis estimates of the appropriate number of spatial degrees of freedom are required. This is necessary, because the number of independent and distinct patterns (types, modes or regimes) often obtained from practical experience, may not be supported by the underlying data sets representing the spatial fields (daily surface pressure maps for Grosswetterlagen, monthly climate mean temperatures and precipitation for climate classifications; see also section 1.2 on representativeness).

Degrees of freedom (spatial embedding): Degrees of freedom (DOF) of a system are estimated from a random sample of state vectors of an M–dimensional space. That is, T observations at M grid points are stored in the $M \times T$ data matrix, $X_i(t_j), i = 1,..,M; j = 1,...,T$. Now, DOF–estimates are obtained by fitting the computed distribution of the standardized χ^2–state variable, $\chi^2_M = \sum_{i=1}^{M}(X_i)^2/M$, to the theoretical χ^2–distribution ($(\chi_{\mathrm{DOF}})^2 = \chi^2/\mathrm{DOF}$, see [1.60]). Using the computed variance $\mathrm{Var}\{\sum_{i=1}^{N} X_i^2\}$ as a sample estimate, the equality $\mathrm{Var}(\chi^2_M) = \mathrm{Var}(\chi^2/\mathrm{DOF})$, and chi–squared distributed variables with mean M and variance $2M$, the degrees of freedom are

$$\mathrm{DOF} = 2M^2/\mathrm{Var}\sum_{i=1}^{N} X_i^2 \,. \tag{1.6}$$

The variance and, therefore, the DOF–estimate can be improved by transformation of the original state variables, $\mathbf{X}(t) = S\Lambda^{1/2}\xi(t)$, to M new independent variables $\xi(t) = \Lambda^{1/2}S^{-1}\mathbf{X}(t)$. They are the projections of the original data sample onto the orthogonal eigenvectors of the symmetric $M \times M$ correlation matrix $C = S\Lambda S^{-1} = \langle \mathbf{X}^* \ \mathbf{X} \rangle$, determined by singular value decomposition of the original $M \times T$ data set $\mathbf{X}(t)$. The matrix Λ contains M eigenvalues λ_i along the main diagonal; the orthogonal matrix S is composed by the eigenvectors of C with $S^{-1} = S^*$ (superscript * denotes the transpose operator). Some algebra finally leads to $\mathrm{DOF} = M^2/\sum_{i=1}^{M}\lambda_i^2$. The relation $M = \mathrm{trace}\ C = \sum_{i=1}^{M}\lambda_i$ shows that the degrees of freedom and the equivalent number of statistically independent observations introduced by Megreditchian [1.40] are identical. In this sense the following DOF–relations can be deduced for the correlation (or covariance) matrices, C (or K), and their respective eigenvalues (λ_c or λ_k); the total variance is $\langle X^2 \rangle = \sum_{k=1}^{M}\lambda_k$. With $(\mathrm{trace}\ C)^2 = (\sum_{c=1}^{M}\lambda_c)^2$ and trace $(C^2) = \sum_{c=1}^{M} \lambda_c^2$ one obtains the degrees of freedom and the confidence limits associated with the correlation (or covariance) matrix C (or K):

$$\mathrm{DOF}(C) = (\mathrm{trace}\ C)^2/\mathrm{trace}\ (C^2)\,, \tag{1.7}$$

$$\Delta\mathrm{DOF} = \nabla(\mathrm{DOF}) \cdot \Delta\lambda = -4\ \mathrm{DOF}\ (2/T')^{1/2}\,. \tag{1.8}$$

Estimates of DOF–confidence limits can be related to those of the eigenvalues λ_m. The rule of thumb derived by [1.47], $\Delta\lambda_m = \pm 2\lambda_m (2/T')^{1/2}$, depends on the number T' of independent realizations. Error–propagation leads to the DOF–confidence limits, where ∇ is the gradient with respect to λ_m. That is, $T' = 1\,000$ independent realizations, corresponding to 10 seasons of daily data with an integral timescale of $\tau = 3 - 4$ days, lead to confidence limits $\mathrm{DOF} \pm \Delta\mathrm{DOF} = \mathrm{DOF}\{1 \pm 4(2/T')^{1/2}\}$, of about 18%. Two applications are presented following Fraedrich et al. [1.21].

Climate zones: Climate classifications follow by two basic principles: *Genetic* classifications consider the influence of the general circulation of the atmosphere (see, for example Flohn and Hupfer [1.11,1.30]), the surface energy fluxes, the tropospheric air masses on climate; further differentiation is possible when utilizing more information: frequency and tracks of cyclones and anticyclones, the intensity and location of quasi–stationary upper troughs, frontal passages, position up– and downstream of mountainous terrain, of coasts, the soil properties which regulate evaporation, albedo etc. *Effective* classifications describe regional climate states by observables and their link with flora, fauna, soil, agricultural use etc. The primary information (or climate elements) on which the effective schemes are based are long term monthly means of temperature and precipitation; threshold values, connected to the vegetation growth, for example, are also included. Such classifications appear to be most suitable for practical applications. A well–known effective scheme has been introduced by Köppen [1.33] which comprises a spatial analysis of the global climate of the continents. Utilizing monthly ensemble means of temperature and precipitation, the Köppen climate regimes are identified by linking maps of vegetation to the climate state variables which leads to world wide main climate zones. With modifications they characterizing the tropical (A), dry (B), subtropical (C), temperate (D), boreal (E), snow (F) climates which are, in parts, subdivided further into wet, summer– and winter–dry, or monsoon–type, oceanic or continental (r, s, w, m, o, c), or tundra and perpetual frost (T, I). The success of this classification lies in its simplicity and its relation to the biosphere; it may be considered as the first step towards a biome oriented analysis of the earth's climate.

The *degrees of freedom* are estimated prior to an application of a classification scheme using monthly means (NCAR 1958–1997) of the near surface temperature and precipitation which, for the European continent, gives DOF

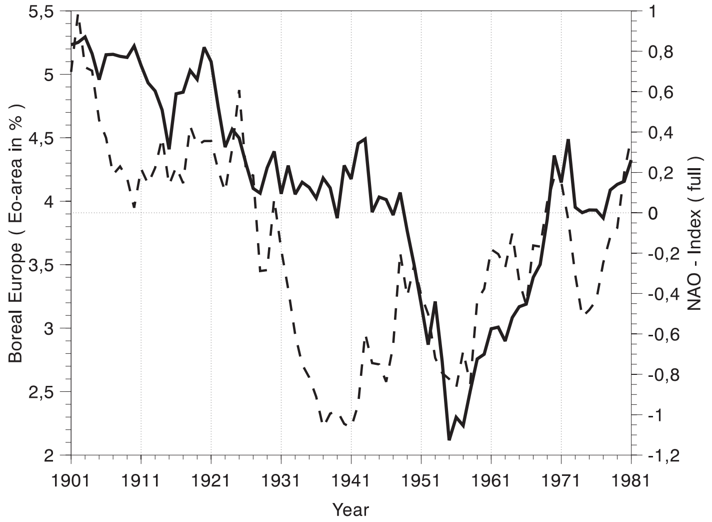

Fig. 1.10. The 1901-95 time series of the North Atlantic Oscillation index (full line) and the relative area occupied by the boreal European Eo-climate (dashed).

= 3. This corresponds with the observed number of climate types employing the modified Köppen scheme: subtropical (C), temperate (D) and boreal (E); the snow–area (F) covers only a small portion of the continent while the dry climate (B) occurs at the south–eastern boundaries in and near Asia. Thus the classification scheme appears to be a useful analysis tool of regional climates and their change analysing the period 1901-95 (Climate Research Unit, University of East Anglia, Norwich [1.46], $0.5° \times 0.5°$ grid resolution): (i) The area cover of the dominating climate zones (Fig. 1.0, in million km^2) is for the subtropical zome (C = 1.5), temperate (D = 8.4), boreal (E = 2.6); snow (F = 0.3) and dry zone (B$\sim$1.4). (ii) A significant correlation between NAO-fluctuations and the European climate zones can only be determined for the area covered by boreal Eo-climate (Fig. 1.10), applying a 15 year averaging window to both the annual NAO index and the surface climate variables entering the classification scheme.

Grosswetterlagen: Grosswetterlagen classifications are introduced to describe the large scale circulation from hemispheric down to regional scales utilizing the evolution of surface pressure fields as the primary information source: (a) The whole Northern Hemisphere extratropics (polewards of 30° N, Dzerdzeevskii [1.9]) is the largest area classified by circulation types (46 including an indeterminable one), which are effectively reduced to 36 individual in summer or winter seasons. These types characterize the hemispheric movements of cyclones and anticyclones which are combined to form 13 elementary circulation patterns which, in turn can be categorized into four principal groups (zonal mean, zonally asymmetric, meridional and mixed). (b) The Grosswetterlagen catalogue characterizes the circulation of the eastern North Atlantic/European sector (Hess and Brezowsky [1.27], [1.23]; Fig. 1.11a) by centres of action lead-

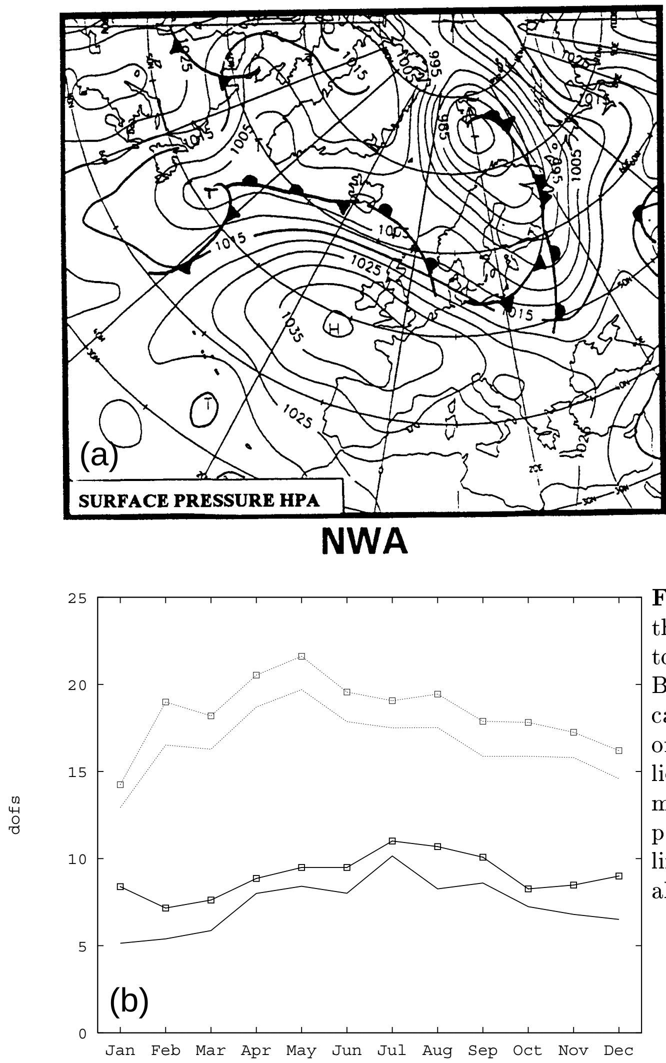

Fig. 1.11. Circulation regimes in the North Atlantic European sector: (a) An example from the Hess-Brezowsky [1.27] Grosswetterlagen catalogue. (b) Estimates of degrees of freedom based on observed anomalies from monthly (squares) and climate means (no squares) using low-pass (full line) and band-pass (dotted line) filtered data (from Fraedrich et al. [1.21]).

ing to 29 (plus one indeterminable) weather types; they are arranged to ten major classes which can be combined to three basic large scale circulation regimes (zonal, meridional and mixed). (c) On a smaller scale (from 50° to 60° N and from 10° W to 2° E) the British Isles weather is based on seven circulation types (Lamb [1.36], see also [1.32]). Other regional classification schemes are also known [1.3]. All catalogues provide long time series of large scale circulation systems identified by often subjective "pattern recognition" applied to the daily surface pressure fields. They have been used, for example, to analyze regime transition probabilities [1.59], to identify far distant teleconnections like the possible link between the ENSO in the tropical Pacific and Europe (Fraedrich, Fraedrich et al. and Wilby [1.13,1.15,1.70]), explain calendar singularities (Bissoli and Schönwiese [1.5]) and climate trends (Werner et al. [1.69]).

A *degree of freedom* analysis is performed prior to a statistical evaluation of North Atlantic/European Grosswetter, utilizing the daily surface pressure field. The data are the geopotential heights of the 1 000 hPa pressure level (ECMWF 1980–1989 with 500 km resolution) which characterize the large scale circulation. The following results are noted (see also Fraedrich et al. [1.21]): (i) The *northern hemisphere* (from 30° to 75° latitude) represented by $M \sim 510$ grid points, yields DOF ~ 30 for unfiltered, DOF ~ 40 for band–pass, and DOF $\sim 15 - 20$ for low–pass filtered data. This corresponds well with the Dzerdzeevskii catalogue identifying 36 different large scale circulation patterns, which are suitably combined to 13 weather regimes. General circulation model simulations with T–21 resolution reveal systematically larger values (plus 5). It appears that the model (although of limited resolution) is not able to generate the sufficiently small number of dominating and active modes which is necessary to adequately simulate the atmosphere's large scale dynamics. (ii) The *North Atlantic/European Sector* with $M \sim 160$ grid points gives, for the unfiltered data, DOF $\sim 10 - 12$; DOF $\sim 7 - 10$ are obtained for low–pass (10–90 days) and DOF $\sim 15-20$ for band–pass (2.5–6 days) filtered data (Fig. 1.11b). These DOF–estimates can be associated with the number of distinct large scale circulation patterns. Hess and Brezowsky [1.27] define 36 Grosswetterlagen for the Atlantic/European sector. This number reduces to 10 Grosswetter–types which corresponds with the low–pass filtered DOF–estimates. The large number of 36 Grosswetterlagen, however, appears to be too large and does not even compare with the band–pass filtered DOFs. In summarizing, the spatial DOFs indicate that the data set analyzed does not allow a resolution of as many details as the large number of phenomenological Grosswetterlagen indicates. Thus, the number of (independent) Grosswetterlagen being substantially larger than the spatial degrees of freedom of the underlying data set requires a considerable reduction of that number to a few regimes, if further statistical analysis is to be employed. Therefore, it is not surprising that analyses of singularities, climate and climate change (as shown in the following) are based on a few regimes only, which comprise dynamically similar Grosswetter types.

The basic *time statistics* of the Grosswetter types describes the North Atlantic/European climate in terms of its synoptic genesis: (i) Three meteorologically distinct large scale circulation regimes are selected. They show that the zonal (or westerly, 31%) and meridional (35%) flow patterns determine the Europe's winter climate, while a set of mixed circulation patterns (34%) can be interpreted as a transition regime with a smaller mean residence time of five days compared to the six and seven day values attained by the zonal and meridional regimes. This interpretation is further supported by the mean first passage time describing regime alternation: 11 or 17 days from meridional to zonal or vice versa, while the transitory mixed state is occupied for about three or five days during the regime passage (see also Spekat et al. [1.59]). (ii) NAO-fluctuations and the North Atlantic/European Grosswetter (in par-

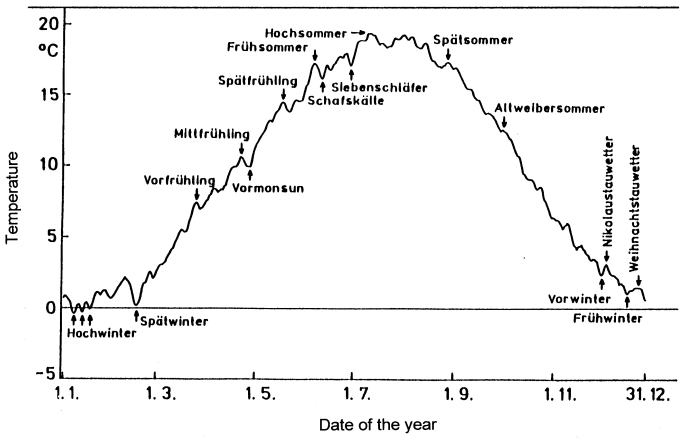

Fig. 1.12. Ensemble mean annual cycle of surface air temperature (1949-85, three-day averages) at Frankfurt/Main; arrows indicate "singularities" with their German names (from Bissoli and Schönwiese [1.5]).

ticular the zonal regime) are closely related. Discarding the common Eulerian frame (of station data), Glowienka ([1.24], [1.48]) introduced a dynamically more relevant Lagrangian NAO index attributed to the changing positions of the mean Icelandic Low and Azores High. In this sense, the flow's seasonal mean occupation times in the zonal (or westerly) Grosswetter state appear to be a more suitable measure of the fluctuating North Atlantic Oscillation than the conventional Eulerian index measure (see section 1.4.1 and Fig.1.14).

1.3.4 Singularities

The annual cycle of, for example, single station surface air temperature at a time resolution of one or a few days (see Fig. 1.12) is not as smooth as may be expected for astronomical reasons (annual cycle of insolation). Particular deviations towards warmer or cooler conditions appear, even after ensemble averaging for many years. These phenomena of more or less regular temperature deviations from the smooth mean annual cycle are called "singularities" (or calendar singularities). Although related to a corresponding behavior of the "Grosswetterlagen" (regimes). There is no steady relation to precipitation. Four types of singularities can be found associated with the following regime change: warm–moist (WM), warm–dry (WD), cold–moist (CM), and cold–dry (CD).

In continental Europe, some of these singularities have been known by experience since a long time, especially in the context of agriculture ("Bauernregeln"), some of them originated in the Roman Empire about two thousand years ago. Traditional German names of singularities are very popular, for instance "Eisheilige" for a CD singularity in May, "Schafskälte" for a CM singularity in June or "Altweibersommer" for a WD singularity near the end of September (corresponding to the "Indian summer" in the USA). Table 1.2 lists some prominent singularities, and their mean calender dates of occurrence and their frequencies.

Type	Date	Frequ. [%]	Type	Date	Frequ. [%]	Type	Date	Frequ. [%]
CD	4.-9.1.	83	CN	24.4.-2.5.	84	WD	25.-26.9.	(76)
CD	13.-14.1.	*	WD	7.-18.5.	95	WD	3.-10.10.	(73)
CD	17.-20.1.	58	CM	20.-31.5.	70	CD	13.-16.10.	87
WM	22.-30.1.	49	WD	2.-8.6.	84	WM	23.-25.10.	*
WM	3.-12.2.	60	CM	10.-12.6.	81	CD	28.10.-1.11.	(76)
CD	14.-20.2.	60	CM	6.-1.7.	70	WM	9.-11.11.	49
CD	27.2.	49	WD	3.-14.7.	89	CD	16.-18.11.	62
CD	7.3.	(76)	CM	16.-24.7.	60	CD	25.-26.11.	87
CD	11.-14.3.	*	WD	28.7.-7.8.	84	WM	27.-28.11.	92
CD	18.-20.3.	(95)	WD	13.-16.8.	*	CD	30.11.-2.12.	(76)
WD	23.-27.3.	62	CM	17.-24.8.	(60)	WM	4.-5.12.	56
WD	3.-4.4.	97	WD	29.8.-5.9.	62	CD	17.-21.12.	53
CD	7.-12.4.	60	WD	11.-12.9.	(81)	WM	24.-29.12.	53
WD	17.-22.4.	73	CM	19.9.	95	CD	4.-9.1.	83

Table 1.2. Type (WM = warm/moist, WD = warm/dry, CM = cold/moist, SD = cold/dry), mean calender data of occurrence and frequency (temperature–related, if not applicable precipitation–related in parentheses) of some Central European "singularities" (simplified from [1.5], observation period 1946–1986, *not significant.)

As every climatic phenomenon, also singularities change in time. For example, Tab. 1.2 does not indicate the CD singularity "Eisheilige", because a statistical analysis shows that, nowadays, this singularity is very rarely occurs and is replaced by a WD singularity around 7–18 May. In contrast to that, based on the 1891–1925 observation period, the CD singularity "Eisheilige" appeared around 6–20 May with a frequency of 97%. Such a change is connected with a regime change of the observed frequency of "Grosswetterlagen".

1.4 Climate Trends: Europe at the End of the Century

The increase of the global mean temperature observed in the last 100 years [1.31] raises two questions: Can signals of climate change be detected in the North Atlantic/European sector and does this change exceed that of the natural variability ? A systematic treatment of climate change requires identification of climate variables or elements which characterize climate states and circulation patterns changing its long term variability. Dynamical processes which are possibly associated with climate change, and indicators, which point to abrupt changes of the atmospheric circulation, need to be found, analyzed and tested. For example, the ice cores in Central Greenland reveal temperature changes of about 7 degrees within a few decades (see [1.10]). Although such abrupt temperature changes have not been observed since the Pleistocene–Holocene transition (after the Younger Dryas), appropriate climatological pa-

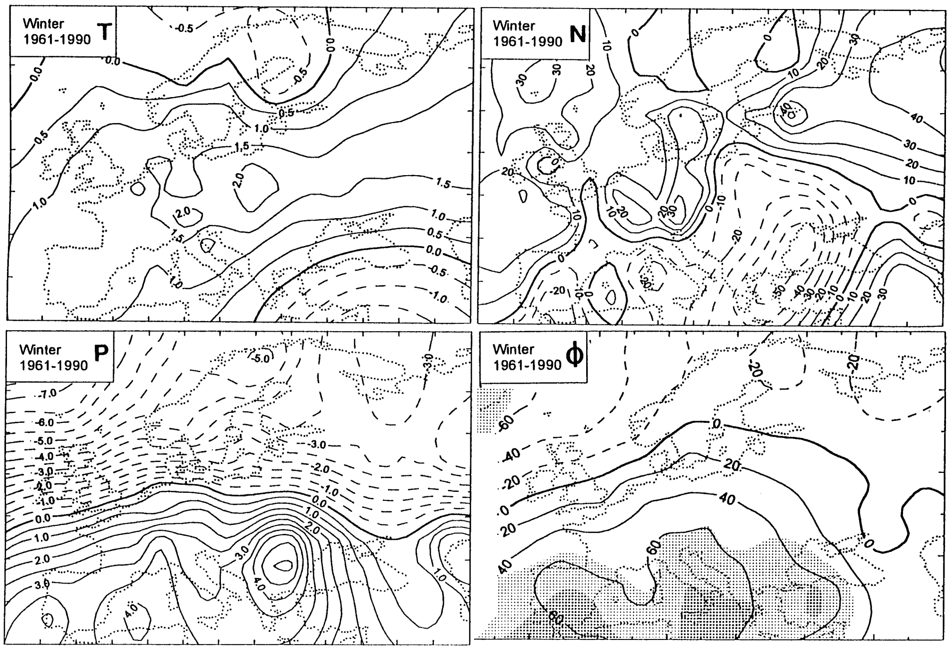

Fig. 1.13. Linear trend patterns (1961-90) in Europe, T = surface air temperature in K, N = precipitation in percent, P = mean sea level pressure in hPa, and Φ = 500 hPa geopotential height in gpm (modified from Schönwiese and Rapp [1.53]).

rameters incorporating the atmosphere's complexity may show such a behavior. For example, the North Atlantic Oscillation (see Figure 1.5, Hurrel [1.28]) reveals decadal fluctuations affecting weather and climate in Europe (Wanner et al. [1.68]). The following sections present analyses of climate trends in Europe at the end of this century utilizing a set of climate elements and indicators which characterize the atmospheric circulation dynamics in a statistically comprehensive manner: Trends of the averages (first moments, section 1.4.1) and of the variability (higher moments, section 1.4.2) are followed by an introduction to the empirical analysis of the external forcing mechanisms.

1.4.1 Trend Patterns of Climate

The climate trend patterns 1961–1990 depending on both season and observation period are indicated concerning changes of the mean fields of the climate elements, surface air temperature, precipitation, mean sea level (MSL) pressure, and 500 hPa geopotential height in Europe (from Schönwiese and Rapp [1.53]). Figure 1.13 shows that, except for northern Scandinavia and the SE Mediterranean area, all regions have experienced warming with maximum values up to 2 K in Central Europe. The precipitation trend pattern is more complicated; the precipitation increase in most areas of West, central and eastern Europe, which is contrasted by a decrease in the Mediterranean area. Note that the most pronounced precipitation decrease (up to 50%) coincides with the maximum of MSL pressure increase. The pressure fields both in MSL and 500 hPa show zonally oriented change patterns with a decrease in the North and an increase in the South (in coincidence with NAO behavior). On a secular time scale the trend patterns for temperature remain similar but not for precipitation and pressure (for details, including confidence tests, see [1.53]).

1.4.2 Storm Tracks and Cyclone Paths; Grosswetterlagen and Climate Zones

Trends of means (that is, monthly, seasonal or annual averages) need to be supplemented by trends of the intrinsic climate variability (second or higher moments) to characterize changes in storm tracks, cyclone densities, residence times of circulation regimes etc., which will be discussed in the following. Note that the effect of the recent changes of the North Atlantic Oscillation (Figures 1.10, 1.5) is also reflected in the trends of stormtracks or cyclone paths, the changing Grosswetterlagen statistics and the shifts of climate zones (see section 1.3.3)

Trends of storm tracks and cyclone paths: The storm tracks trends are determined by the slope of a linear regression normalized per decade during 1979–1997. The North Atlantic storm track shifts to the Northeast, and, over Europe, the variability is displaced eastwards (Fig. 1.7b). The trend of the cyclone density (Fig. 1.9b) shows a north–eastward shift with a decrease in the western Atlantic and an increase over Scandinavia, which is very similar to the storm track trend (Fig. 1.7b). The reduction of the storm track over central Europe can be found in the trend of the cyclone density. In eastern Europe, however, the enhancement of the storm track is not due to cyclone density, which shows a distinct decrease in this area (see change of climate zones Fig. 1.9b). Note that, simultaneously with the north–eastward shift of the cyclone density, the numbers of short–lived cyclones (without minimal lifetime, hence including lows which exist only one time step) and the cyclones with at least 3 days life time decrease both with a rate of about 2 per decade (see [1.56]).

Changing Grosswetterlagen statistics (frequency and residence time): The variability associated with the climate of the North Atlantic/European sector is suitably described in terms of large scale circulation regimes. Characterizing the underlying dynamics requires appropriate measures of the variability which are useful climate signals to identify trends and abrupt changes. Here, the statistics of the occupation time (frequency) or residence time (duration) will be applied, first to two univariate regimes (the cold– and the warm–type regimes) and then to a binary process (the zonal flow regime and its complement comprising all remaining other Grosswetter types). A trend analysis of the *frequency or occupation time* of warm– and cold–type Grosswetterlagen is summarized in Tab. 1.3. It reveals that in summer and winter a frequency increase of the warm regime is observed, corresponding to a decrease of the cold regime. This change is very pronounced in summer (47% increase of warm–type–Grosswetterlagen).

Period	Summer, W [%]	Summer, C [%]	Winter, W [%]	Winter, C [%]
1901-1930	31.6	51.0	39.3	27.1
1931-1960	40.4	49.3	35.8	33.3
1961-1990	46.7	42.3	43.1	31.2

Table 1.3. Frequency of relatively warm– and cold–type European Grosswetterlagen (W or C) in summer and winter (from Hupfer and Schönwiese [1.29]).

Residence times characterize the persistence of circulation regimes of, for example, the zonal Grosswetter, which is closely associated with the cross Atlantic storm track (see Figs. 1.4, 1.7, 1.9) and, due the existence of the Gulf stream, determines the temperate climate of the European continent (see Fig. 1.0). Confining the dynamics to a dichotomous (or binary) process of two circulation states, the zonal regime $Z(t)$ and its complement (no Z), decadal mean residence times of the state Z can be estimated; it shows an abrupt increase near the beginning of the seventies (Fig. 1.14a,b). An outlier test (Thompson rule, see Müller et al. [1.45]) of this climate signal (decadal winter mean duration of the zonal regimes) identifies the 1981-1990 decade as the onset of climate change in the North Atlantic/European sector; the trend commences in the beginning of the seventies. Beyond that decade the observed peaks do not belong to the previous centennial sample (1881–1980) on the 99% significance level (denoted by triangles). The observed climate change in the North Atlantic/European sector can be attributed to the surface temperature anomalies of the Earth's continents and to the increasing intensity of the North Atlantic Oscillation (see Figure 1.5. Their decadal sequences from 1901 to 1997 show simultaneous rise from the 1971–1980 decade onwards, which is another indication of a global climate mode. It describes the "warm continent – cold ocean" state (and vice versa) dominating the end of this century. Other parameters (ENSO variability, North Atlantic sea surface temperatures, Northern Hemisphere temperatures) have been excluded to be significantly related to the observed climate change in Europe (see Werner et al. [1.69], for more details). Applying the same analysis to the Lamb circulation patterns, that is, the type 16 (west) plus 26 (cyclonal west), leads to the same results (not shown). Another support comes from an analysis of Central European Grosswetter, precipitation, and temperature (Bardossy and Caspary [1.2]). Furthermore, the mean occupation times of the circulations states reveal an analogous time

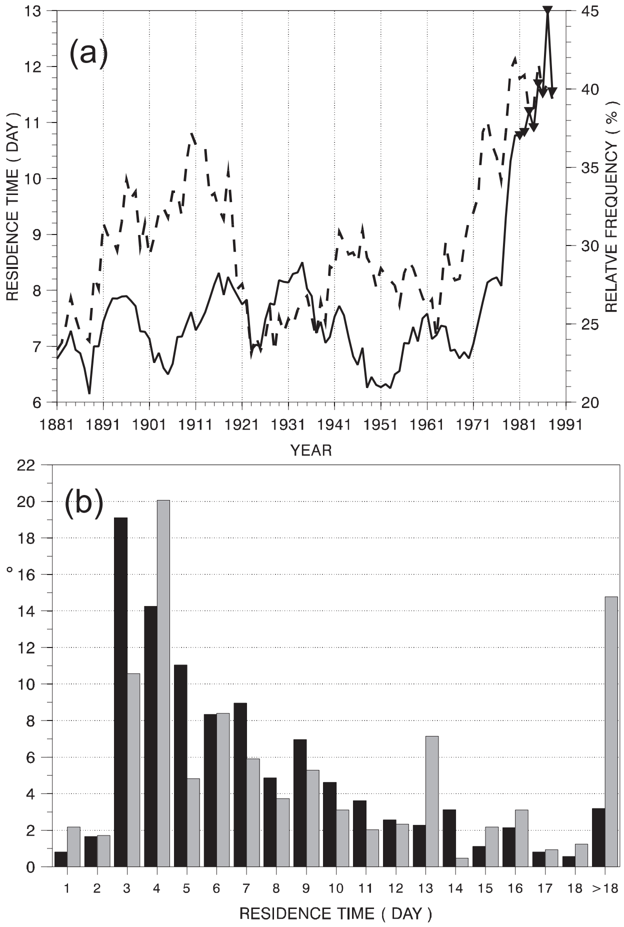

Fig. 1.14. (a) Time series of the decadal means of the residence times (full line, left axis) and occupation time (dashed, right axis) of the zonal (or westerly) Grosswetter state in winter (1881/82 - 1997/98); triangles define statistically safe outliers (β= 0.05); (b) residence time distributions (relative frequencies) for periods 1881 to 1970 (black columns) and 1971 to 1997 (grey; from Werner et al. [1.69]).

evolution but there are no statistically safe outliers on the required level of significance.

Shift of climate zones: The analysis of the climate classification scheme (from 1901 to 1995, see section 1.3.3) is extended to the changes occurring near the end of this century. Shifts observed during the last 15 years are presented in Figure 1.0 (covering a 30 year span by the sliding 15 year window, after Fraedrich et al. 2001 [1.22]). It appears that Europe realises the largest change of climate zones (relative to its area) compared with all other continents. Here it is the maritime temperate climate (Do) which increases its area by 289 $10^3 km^2$ replacing mainly the continental climate (Dc), which looses 222 $10^3 km^2$.

1.4.3 External Forcing: Natural and Anthropogenic

External forcing mechanisms of the climate system are defined to operate without direct interactions. They can be identified in terms of radiation anomalies (radiative forcing) within the atmosphere surface subsystem leading to the corresponding temperature effects as they are simulated, for example, by energy balance models. However, they are also involved with indirect effects, often due to modifications caused by a change of the atmospheric composition (cloud effects) and circulation. This indirect forcing, which involves the response of all climate elements, is very uncertain and a matter of continuing research.

Causes: For example, explosive *volcanism* effects climate anomalies of a few years but climate change does not trigger volcanic eruptions (as far as we know). The climatic effect is that the additional volcanogenic aerosol layer which has a typical residence time of $1 - 3$ yr after eruption, absorbs and scatters some part of the solar irradiation, leading to a warming of the stratosphere, whereas the insolation transmission into the lower part of the atmosphere (troposphere) is decreased leading to cooling effects near the Earth's surface. This radiation forcing which is dominated by sulfate particles can be quantified. Following [1.41] the tropospheric radiation forcing was 2.4 Wm^{-2} in the year of the Pinatubo eruption (1991), 3.2 Wm^{-2} one year later (maximum effect) and 0.9 Wm^{-2} two years later. For earlier decades without direct observation of the stratosphere such assessments are not possible. However, some authors have tried to evaluate annual explosive volcanism parameter time series where this parameter is based on historical volcanoe chronologies (such as by [1.57]. One of the most recent assessments used in the following is from [1.26]) where both sulfate particle building via gas–to–particle conversion and sedimentation are taken into account.

Solar forcing of climate is a matter of controversial discussion since a long time. On a decadal to secular time scale the question has to be answered whether solar activity by solar flares etc. and indicated by sunspots has a significant influence on climate or not. Based on a number of recent publications [1.31]) states a fluctuative forcing of $0.1 - 0.5$ Wm^{-2} where the related time series mostly are closely related to sunspot relative numbers (SRN, see [1.12]). So SRN time series may be used as a solar forcing proxy. Alternatively, solar forcing may have been also contributed to a secular trend [1.38], however, at a similar magnitude as quantified above. We use this assumption, too. All other solar hypotheses, e.g. concerning an influence of the length of the solar cycle or solar diameter variations seem to be speculative (Schönwiese et al. [1.55]).

Anthropogenic sources provide the most important secular forcing of global relevance. It is due to the emission of greenhouse gases (GHG: CO_2, CH_4, CFC, N_2O, tropospheric O_3 etc.) in the context of human activities like energy use, traffic, deforestation, agriculture and some other. This problem was described and discussed at length by [1.31]). The most important point is that the corresponding atmospheric concentration increase since approximately 1850 (not only due to CO_2 but so–called CO_2 equivalents) is quantified as a $2.1 - 2.8$ Wm^{-2} radiative forcing and that in case of a CO_2 doubling (4.4 Wm^{-2} forc-

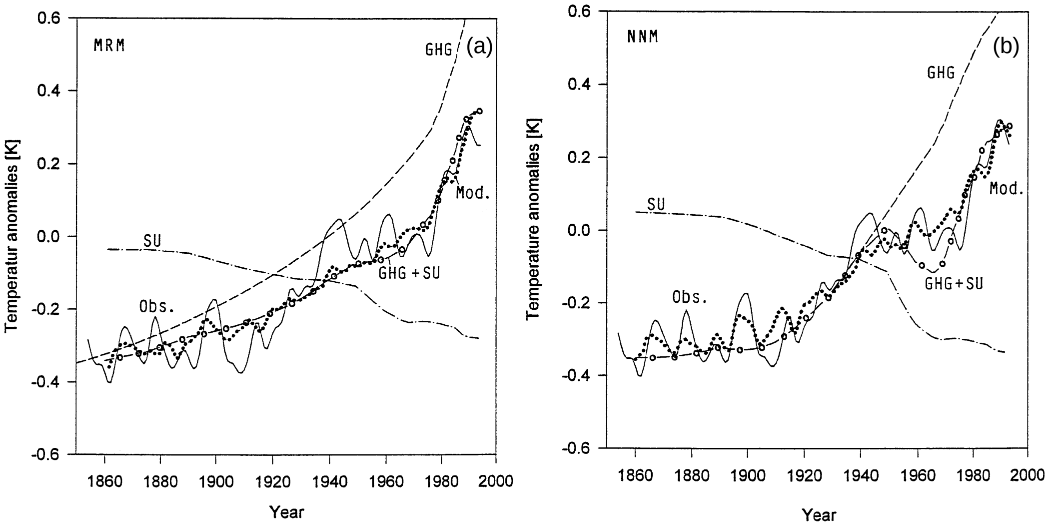

Fig. 1.15. (a) Observed global mean surface air temperature anomalies 1854-1994, 10 yr low-pass filtered (data from [1.31]), solid line, reproduction by means of a multiple regression model (MRM) using greenhouse gas (GHG), sulfate aerosol (SU, both anthropogenic) such as volcanic, solar, and ENSO forcing, dotted line, in addition related GHG (dashed line) and SU (dashed-dotted line) signal time series (from [1.52]). (b) As in (a) but neural network model (NNM, backpropagation) simulation.

ing) a global mean surface air temperature increase of 2.1 – 4.6 K (equilibrium response) is simulated by coupled atmosphere–ocean circulation models (AOGCM, [1.31]). The same models attribute to this forcing so far roughly 1 K temperature increase (transient response, i.e. time lags implied). A second anthropogenic but negative forcing is due to tropospheric sulfate aerosol particles (SUA) which may have lead to a cooling of approximately 0.4 – 0.6 K during the same industrial time and as simulated by AOGCM as well [1.31]. Figure 1.15 shows the time series of all natural and anthropogenic forcing mechanisms mentioned above and related to in the following (including ENSO using the Southern Oscillation Index SOI).

Effects: Statistical techniques are used to check how much of the observed surface air temperature variance can be reproduced by a combination of GHG, SUA, volcanic, solar and ENSO forcing. It arises that a simple multiple regression model MRM (logarithmic GHG–temperature relationship, all other relationships are linear; the GHG–temperature time lag of 20 yr has been assessed by cross correlation analysis; the volcanic delay is 1 yr and all other forcings are without delay) is able to explain 73% of this variance on a global mean annual basis. A neural network model (NNM, backpropagation architecture; [1.58]) which is trained to fit non–linear relationships (and allows forcing factor interactions) comes out with 83%. The next step is to try to attribute particular isolated forcing factors to observed variation components (the sum of these components or climate "signals" is the total variance explained). The results of this signal analysis are very similar in case of MRM and NNM and proportional to the radiative forcing postulated by [1.31], (see also Tab. 1.4).

Influence	Forcing [Wm^2]	NNM [K]	MRM [K]	Time structure
Greenhouse gases (GHG)	+ 2.1–2.8	0.9–1.3	0.8–1.2	non-linear trend
Sulfate aerosols (SUA)	- 0.4–1.5	0.2–0.4	0.1–0.4	non-linear var. trend
Combined (GHG + SUA)	+ (0.6–2.4)	0.5–0.7	0.6–0.8	non-linear var. trend
Volcanism (VIG)	- 1.0–3.0*	0.1–0.2	0.1–0.4	episodic (1–3 yr)
Solar activity (SRN)	+ 0.1–0.5	0.1–0.2	0.1–0.2	fluctuative (+ trend?)
El Niño (ENSO)	+ (internal)	0.2–0.3	0.2–0.3	episodic (0.5 yr)
CO_2 doubling, equilibrium	+ 4.4**	2.1	2.6–3.9	non-linear trend
CO_2 doubling, transient	+ 4.4**	1.7	1.8–2.6	non-linear trend
Explained variance		83%	73%	annual data

Table 1.4. Global mean tropospheric radiative forcing of the specified influence factors since approximately 1850 (from [1.31]) and related surface air temperature signals as assessed by neural network and multiple regression models (NNM and MRM [1.52,1.54,1.67]; *only after major eruptions like Pinatubo: 1991 → 2.4, 1992 → 3.2, 1993 → 0.9 Wm^{-2} [1.41]; **GCM [1.31]: equilibrium 2.1–4.6 K; transient 1.3–3.8 K).

On a regional-seasonal scale the statistical signal assessments suffer from a very low amount of explained variance. Nevertheless, some preliminary results for Europe, from a related MRM analysis, are listed in Tab. 1.5. Note that in this case the maximum GHG signals are found in summer. However, in line with the small amount of explained variance, the observed trends and the simulated signal sums differ considerably. In case of related NNM signals some strange results arise which seem to contradict the physical background. It appears that the neural network technique fails to reproduce reasonable signal results if the total amount of explained variance is relatively small.

Influence	Spring [K]	Summer [K]	Autumn [K]	Winter [K]	Year [K]
Greenhouse gases (GHG)	1.2	1.4	1.2	0.8	1.2
Sulfate aerosols (SUA)	-0.6	-0.9	-0.7	-0.3	-0.6
Combined (GHG + SUA)	0.7	0.5	0.5	0.5	0.6
Sum of all signals simulated	0.7	0.5	0.5	0.5	0.6
Observed trends	0.4	0.2	0.3	0.4	0.4
Explained variance (MRM)	20%	23%	18%	11%	28%
MRM prediction 1991-2040 *	1.7	2.0	1.7	1.1	1.7
OAGCM prediction 1935-2084 *	1.9	2.2	1.9	3.6	2.3

Table 1.5. Statistical assessments of anthropogenic European surface air temperature signals 1892–1991 and related predictions using MRM (multiple regressions) or OAGCM (ocean atmosphere general circulation models) from [1.54]; * GHG trend scenario IS90A, "business–as–usual" [1.31]; OAGCM from [1.8]).

1.5 Conclusion

The space–time variability of the European climate is analyzed which, due to its position at the tail end of the North Atlantic storm track, depends strongly on the oceanic circulation. This privileged situation allows Europe to support a population of 300 million people polewards from the 40°N latitude circle which, compared to the 30 million people living in North America or Eastern Asia north of the same latitude, is unique for the Earth. Europe's climate analysis described in this review follows four steps employing both physical observations and phenomenological data sets:

The *first* step characterizes the climate by the spatial distributions of long term means and variances of the fundamental physical climate elements (surface air temperature, sea level pressure, and precipitation).

The *second* step requires the analysis of the underlying processes generating the climate. In the European sector these are the rain bearing frontal systems which, in terms of cyclone paths (densities) and storm tracks, create dynamically meaningful quantitative climatologies employing Lagrangian and Eulerian analyses of weather maps. The analysis of the climate generating processes is supplemented by the statistics of qualitative phenomenological patterns (or regimes) like Grosswetterlagen and climate zones which embed the regional climate into its geographical and biospheric environment.

The climate state associated with its space–time variability may undergo long term changes associated with global change of natural or anthropogenic origin; this constitutes the *third* step of climate analysis. The climatologies described above document a recent climate change at the end of this century after employing trend analyses of the spatial distribution of time averaged climate elements and of various measures of their variability (storm tracks or second moments and cyclone densities, occupation and residence times of circulation regimes).

The *fourth* and final step consists of an analysis of the climate trend generating processes. Dynamical models or empirical analyses (the latter approach is adopted here) are used to determine the effects of external forcing of the climate due to volcanism, solar variability, and anthropogenic activities.

Acknowledgments:. The authors gratefully acknowledge F.-W. Gerstengarbe, P.C. Werner and P. Hupfer for the continuing discussions, cooperation, and support on the climate and climate change issues raised in this paper.

References

1.1 C. Appenzeller, T. F. Stocker and M. Anklin, Science, **282**, 446 (1998).
1.2 A. Bardossy and H. J. Caspary, Theor. Appl. Climatol. **42**, 155 (1990).

1.3 R. G. Barry and A. H. Perry (eds.), *Synoptic Climatology, Methods and Applications* (Methuen & Co Ltd., London, 1973), p. 555.
1.4 P. Bissolli and C. D. Schönwiese, Meteorol. Rundsch. **40**, 147 (1987).
1.5 P. Bissolli and C.-D. Schönwiese, Naturwiss. Rdsch. **44**, 169 (1991).
1.6 M. L. Blackmon, J. Atmos. Sci. **33**, 1607 (1976).
1.7 R. Blender, K. Fraedrich, and F. Lunkeit, Q. J.R. Meteorol. Soc. **123**, 727 (1997).
1.8 U. Cubasch, G. C. Hegerl, A. Hellbach, H. Hoeck, U. Mikolajewicz, B.D. Santer, and E. Voss, Clim. Dynamics *11*, 71 (1995).
1.9 B.L. Dzerdzeevskii (ed.), *The Observed Circulation of the Atmosphere and Climate* (Moscow, 285, 1975).
1.10 W. Dansgaard, J.W.C. White, and S.J. Johnsen, Nature **339**, 532 (1989).
1.11 H. Flohn, Erdkunde **4**, 141 (1950).
1.12 P. V. Foukal and J. Lean, Science **247**, 556 (1990).
1.13 K. Fraedrich, Intern. J. Climatol. **10**, 21 (1990).
1.14 K. Fraedrich and K. Müller, Intern. J. Climatol. **12**, 25 (1992).
1.15 K. Fraedrich, E.R. Kuglin, and K. Mueller, Tellus **44A**, 33 (1992).
1.16 K. Fraedrich, C. Bantzer, and U. Burkhardt, Climate Dynamics **8**, 161 (1993).
1.17 K. Fraedrich and C. Larnder, Tellus **45A**, 289 (1993).
1.18 K. Fraedrich, Tellus **46A**, 541 (1994).
1.19 K. Fraedrich, R. Bach, and G. Naujokat, Contr. Atmos. Phys. **59**, 54 (1986).
1.20 K. Fraedrich and L.M. Leslie, Q.J.R. Meteorol. Soc. **115**, 79 (1989).
1.21 K. Fraedrich, C. Ziehmann, and F. Sielmann, J. Climate **8**, 361 (1995).
1.22 K. Fraedrich, F.W. Gerstengarbe and P.C. Werner, Climate Change **45** (2001).
1.23 F. W. Gerstengarbe and P.C. Werner, Berichte des Deutschen Wetterdienstes **113**, 249 (1993).
1.24 R. Glowienka, Contr. Atmos. Physics, **58**, 160 (1985).
1.25 E. J. Gumbel, *Statistics of Extremes*, (Columbia University Press, 1958).
1.26 J. Grieser and C.-D. Schönwiese, Atmosfera **12**, 111 (1999).
1.27 P. Hess and H. Brezowsky, Berichte des Deutschen Wetterdienstes **15**, 54 (1977).
1.28 J. W. Hurrel, Science **269**, 676 (1995).
1.29 P. Hupfer and C.-D. Schönwiese, Wiss. Auswertungen + GEO, Hamburg, **99** (1998).
1.30 P. Hupfer (ed), *Das Klimasystem der Erde* (Akademie-Verlag, Berlin, 464, 1991).
1.31 IPCC, *Climate Change* (Cambridge University Press, Cambridge, 1996), p. 572.
1.32 P.D. Jones, M. Hulme, and K.R. Briffa, Int. J. Climatol. **13**, 655 (1993).
1.33 W. Köppen, *Das geographische System der Klimate* (Bornträger Verlag, Berlin, 1936).
1.34 W. Köppen, Mitteilungen der Geographischen Gesellschaft in Hamburg **1**, 76 (1881).
1.35 J.E. Kutzbach, J. Appl. Meteorol. **6**, 791 (1967).
1.36 H.H. Lamb, Geophys. Mem., 116, HMSO, London, 85 (1972).
1.37 N.C. Lau, J. Atmos. Sci. *45*, 2718 (1988).
1.38 J. Lean, J. Beer and R. Bradley, Geophys. Res. Letters **22**, 3195 (1995).
1.39 J. Malcher and C.-D. Schönwiese, Theor. Appl. Climatol. **38**, 157 (1987).
1.40 G. Megreditchian, Computational Statistics & Data Analysis **9**, 57 (1990).
1.41 M.P. McCormick, L.W. Thomason, and C.R. Trepte, Nature **373**, 399 (1995).
1.42 J. M. Mitchell, B. Dzerdzeevskii, H. Flohn, W.L. Hofmeyr, H.H. Lamb, K.N. Rao, and C.C. Wallen, WMO Tech. Note **79**, Geneva, 79 (1966).
1.43 J.M. Mitchell, *Das Klima. Analysen und Modelle - Geschichte und Zukunft* (Springer Verlag, Berlin, 1980), p. 296.
1.44 F. Molteni and S. Tibaldi, Q.J.R. Meteorol. Soc. **116**, 1263 (1990).
1.45 P.H. Mueller, P. Neumann, and R. Storm, *Tafel der mathematischen Statistik* (VEB Fachbuchverlag, Leipzig, 1973).
1.46 M. New and M. Hulm, Physics of Climate Conference, R. Meteorol. Soc., London, (1997).
1.47 G. R. North, T.L. Bell, R. F. Cahalan, and F. J. Moeng, F.J., Mon. Wea. Rev. **110**, 699 (1982).
1.48 H. Paeth, A. Hense, R. Glowienka-Hense, R. Voss, U. Cubasch, Climate Dynamics, **15**, 953 (1999).
1.49 L. F. Richardson, Proc. Roy. Soc., London, **A110**, 709 (1926).
1.50 B. Saltzman, Adv. in Geophysics **25**, 173 (1983).
1.51 B.G. Sanderson and D.A. Booth, Tellus **43A**, 334 (1991).

1.52 C.D. Schönwiese, M. Denhard, J. Grieser, and A. Walter, Theor. Appl. Climatol. **57**, 119 (1997).
1.53 C. D. Schönwiese and J. Rapp, *Climate Trend Atlas of Europe - Based on Observations* (Kluwer, Dordrecht, 1997), p. 228.
1.54 C. D. Schönwiese, A. Walter, J. Rapp, S. Meyhöfer and M. Denhard, Bericht 102, Inst. Meteorol. Geophys. Univ. Frankfurt/Main, 156 (1998).
1.55 C.-D. Schönwiese, R. Ullrich and F. Beck, Clim. Change **27**, 259 (1994).
1.56 M. Sickmöller, R. Blender and K. Fraedrich, Q. J. R. Meteorol. Soc. **126**, 1 (2000).
1.57 T. Simkin, L. Siebert, L. McClelland, D. Bridge, C.G. Newhall, and J.H. Latter (eds.), *Volcanoes of the World* (Hutchinson, Stroudsbourg (and unpublished updates), 1981), p. 232.
1.58 M. Smith, *Neural Networks for Statistical Modelling* (Van Nostand Reinhold, New York, 1993), p. 235.
1.59 A. Spekat, B. Heller-Schulze, and M. Lutz, Meteorol. Rdsch. **36**, 243 (1983).
1.60 Z. Toth, Tellus **47A**, 457 (1995).
1.61 A. Tsinober, Non-linear Processes in Geophysics **1**, 80 (1994).
1.62 R. Vautard, Mon. Wea. Rev. **118**, 2056 (1990).
1.63 J.A. Viecelli, J. Atmos. Sci. **51**, 337 (1994).
1.64 H. von Storch and F.W. Zwiers, *Statistical Analysis in Climate Research* (Cambridge University Press, Cambridge, 1999), p. 484.
1.65 J. M. Wallace, X. Cheng, and D. Sun, Tellus **43A**, 16 (1991).
1.66 J. M. Wallace and D. S. Gutzler, Mon. Wea. Rev., **109**, 782-812 (1981).
1.67 A. Walter, M. Denhard, and C.-D. Schönwiese, Meteorol. Z. **NF7**, 171 (1998).
1.68 H. Wanner, R. Rickli, E. Salvisberg, C. Schmutz, *Klimawandel im Schweizer Alpenraum* (Hochschulverlag AG der ETH Zürich, Zürich, 2000), p. 285.
1.69 P.C. Werner, F.-W. Gerstengarbe, K. Fraedrich. and H. Oesterle, Int. Jour. Climatol. **20**, 463 (2000).
1.70 R. Wilby, Weather **48**, 234 (1993).